Hindawi Publishing Corporation
Advances in Mechanical Engineering
Volume 2014, Article ID 693592, 15 pages
http://dx.doi.org/10.1155/2014/693592

Research Article

Energy Harvesting Shock Absorber with Electromagnetic and Fluid Damping

Nitin V. Satpute,[1] Shankar Singh,[2] and S. M. Sawant[3]

[1] *Mechanical Engineering Department, Vishwakarma Institute of Technology, 666 Upper Indiranagar, Bibwewadi, Pune, Maharashtra 411037, India*
[2] *Sant Longowal Institute of Engineering and Technology, Longowal, Sangrur District, Punjab 148106, India*
[3] *Rajarambapu Institute of Engineering and Technology, Sakharale, Sangli District, Maharashtra 415414, India*

Correspondence should be addressed to Nitin V. Satpute; nitinsatpute123@gmail.com

Received 6 November 2013; Revised 7 February 2014; Accepted 16 February 2014; Published 17 April 2014

Academic Editor: Anand Thite

During the last two decades, attempts have been made by researchers to build integrated suspension/generation unit that can replace conventional fluid shock absorbers in vehicles. However, heavier weight is limiting commercial application of the present systems. This paper presents design and analysis of an efficient energy harvesting hydraulic electromagnetic shock absorber with least weight penalty on the vehicle. The conceived shock absorber uses mechanical amplification and linear generator along with displacement sensitive fluid damper. Prototype linear generator operating with velocity amplification improves harvested voltage to 660%. Full scale model of the presented system will harvest peak energy of 176–227 J for suspension velocities of 0.25–0.40 m/sec. Finite element analysis in ANSYS is used to derive optimum generator dimensions. Numerical model of the present system with fluid and electromagnetic damping has been constructed in Matlab Simscape. Inductive voltage drop and harvesting threshold voltage are found to contribute nonlinearity of the electromagnetic damping force. Quarter car model constructed in Matlab is used to evaluate motion transmissibility, acceleration transmissibility, and wheel motion. Satisfactory performance of the system is confidently validated with experimentations performed on a scaled-down prototype.

1. Introduction

Increased emission of greenhouse gases has made automobile manufacturers focus on energy efficient, low emission, and even solar/hybrid vehicles. Kinetic energy dissipated in vehicle shock absorbers is one of the important losses apart from braking and thermal efficiency.

Published literature identifies that the applications of electrical generators in vehicle suspension have been investigated for more than two decades. Oprea et al. have explained theoretical framework for using linear generator as a damper in vehicle shock absorber [1]. Finite element simulations are used to determine the generator dimensions for maximum flux density in slotless windings. In order to optimize the configuration, authors suggested evaluation of various machine configurations with different magnet and pole thickness. Design of linear generator with rare earth magnets for use in an automobile suspension has been discussed by Zuo et al. [2]. Zhen and Wei have analyzed structure of linear generator for a vehicle weighing 1.3 tons [3]. It has been calculated that maximum damping force of 1145 N can be reached by the linear generator with car vertical velocity of 0.17 mm/sec. However, work does not demonstrate model of the linear generator fabricated to verify the calculations. Application of an electromagnetic damper in active suspension system is demonstrated by Kawamoto et al. [4]. An electric motor is used to apply active force with use of ball screw arrangement. Self-powered active vibration system proposed by Nakano et al. operates with regenerated energy [5]. Authors have validated that the presented system can run with zero average power consumption. Ebrahimi et al. have presented equations to estimate overall dimensions of the generator for maximum damping force [6]. Simulations performed with the numerical model estimated maximum damping coefficient to be 950 kg-m/sec. A linear generator with fourfold increase in air gap magnetic flux density has

been patented by Goldner and Zerigian [7]. In his doctoral thesis, Zador has used finite element analysis and numerical modeling to optimize damping force of the linear generator [8]. Optimization results show that with use of rare earth magnets, maximum reaction force of 4000 N can be achieved for relative velocity of 0.7 m/sec. Ohashi and Matsuzuka have observed that amplitude of the voltage generated by linear synchronous generator is inversely proportional to the square of frequency [9]. Paz has discussed several designs of linear generator for use in automobile shock absorber [10]. Calculation results presented by the author show that the linear generator can harvest up to 40% of the vibration energy lost in vehicle shock absorber.

Regenerative shock absorber proposed by Li et al. has several components including dc generator, planetary gear box, bevel gears, and rack-pinion [11]. Authors have observed that damping performance of the shock absorber depends on the electrical load resistance. Amati et al. have proposed use of shunted permanent magnet motor and ball screw for building lighter weight electromagnetic shock absorber [12]. Authors have noticed up to 33% variation in the damping force for 5 Ω change in load resistance. Fang et al. have investigated energy recovery characteristics of hydraulic electromagnetic shock absorber [13]. Hydraulic motor, accumulator, and check valves were used to drive an electric generator. With energy recovery efficiency of 16.6%, the presented system reported peak energy of 200 W at 10 Hz. Zhang, using double layered configuration of the linear generator, increased power generation by eight times and energy density by a factor of 5, compared with performance of single layer configuration [14]. Liu and Lin have estimated that maximum power generation of 12 W can be achieved from each of a car shock absorber, with the use of tubular permanent magnet linear generator [15]. Authors have changed the damping effect of the generator by varying load resistance. Energy harvested by the linear generator was found to be different under harmonic and broadband excitations [16].

Ouyang et al. have achieved motion amplification up to 7.82, with the use of double symmetric compliant mechanisms [17]. An electromagnetic energy harvester operating with variable stiffness has been proposed by Hadas et al. [18]. The device operates a wireless application with energy harvested from ambient vibrations. Zeimpekis et al. have used micromachined lever mechanism to achieve motion amplification up to 40 times [19]. Design of scissor jack motion amplification mechanism has been discussed by Huang and McNamara [20]. A viscous damper operating with the amplified motion has shown significant improvement in damping efficiency.

Damping coefficient and stiffness of shock absorber are chosen for acceptable ride quality and wheel motion. Higher values of damping coefficient and spring stiffness are recommended for driver's oscillatory comfort up to 1.5 Hz [21]. However, lower values of the two are recommended at frequency lower than 1.5 Hz. Zhou et al. have determined dimensions of the throttle area for design damping coefficient of the fluid shock absorber [22]. Authors have analyzed the effect of these dimensions on the damper performance with an analytical model.

Although many researchers have developed energy harvesting shock absorber, few concerns still remain to be addressed. With the use of linear generator, frequency of the generated voltage waveform is different than the excitation frequency [1, 2]. This leads the damping force frequency to differ from the excitation frequency, which will give On-Off effect on the electromagnetic damping force. This aspect has not been investigated by many authors. Finite element (FE) analysis has been performed to maximize flux density in the linear generator [2, 15]. However, effect of magnet and pole dimensions on energy dissipated by the generator has not been studied.

For a fluid damper, flow clearance area and cracking pressure of the valves decide damping coefficient, which is fairly linear [23]. However, effect of armature coil parameters and electrical load on mechanical nonlinearity of the electromagnetic damping coefficient still needs to be investigated. Electromagnetic damping force significantly depends on electrical load [11]. Energy harvested from shock absorber can be used for some useful application like battery charging. With linear generator as the only dissipative element in the shock absorber, damping coefficient will significantly change with variation in the load resistance. Possibility of zero damping force in case of armature winding or supporting hardware failure is one of the major drawbacks of the present systems. These aspects necessitate the use of fluid damper as additional dissipative element in an energy harvesting shock absorber. Design damping coefficient of fluid damper that can be used along with the linear generator has not been discussed by the previous researchers.

Heavy structure of present electromagnetic shock absorbers is limiting their commercial application [7, 13]. Attempts are being made to build lighter energy harvesting shock absorbers with the use of rotary generator. Ball screw arrangement or rack and pinion is used to convert linear motion into rotary [11, 12]. For increasing transmission ratio a number of helical and bevel gears are also included in the system. Ball screw harvester gives poor performance at higher frequencies [24]. Presence of backlash and possibility of cracks seriously affect reliability and durability of regenerative shock absorbers with mechanical gears. Also the use of the number of elements along with gears affects dynamics of the system, thereby increasing cost and limiting harvesting efficiency.

The major design focus of this research article is to develop an energy efficient suspension/generation unit that can replace conventional fluid shock absorber in vehicles without increased weight penalty. The present paper highlights the design and validation of hydraulic electromagnetic shock absorber (HESA). Mechanical linkage mechanism used in the shock absorber operates the horizontally located linear generator with improved efficiency. Based on the dynamic simulation of detailed numerical model, performance characteristics of HESA (displacement, force and acceleration transmissibility, braking force on coils, harvested electrical energy, and damping coefficient) have been investigated. This numerical model characterizes the electromechanic parameters of the generator in terms of dimensions, coil parameters, and electric load. Nonlinear nature of

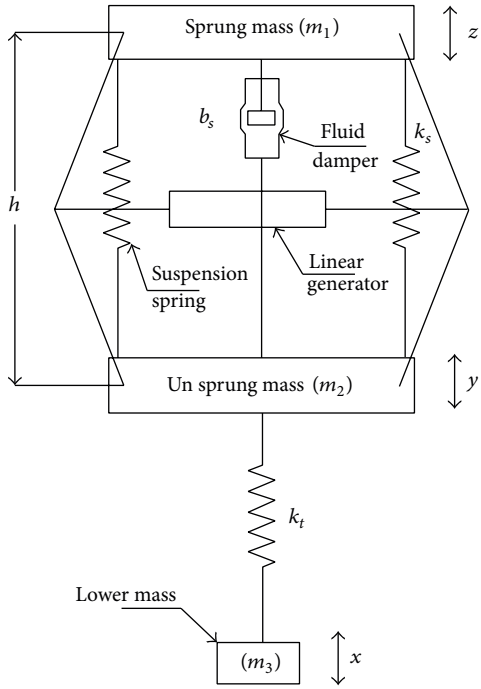

Figure 1: Arrangement of HESA and quarter car model.

the electromagnetic damping coefficient has been highlighted with discussion on factors affecting the nonlinearity. Since vehicle vibrations are seldom harmonic, presented shock absorber is analyzed under broadband excitations.

Numerical model of prototype HESA has been validated with experimental test results on a scaled-down prototype. Finally, the design and analysis of full scale shock absorber with the use of rare earth magnets have been presented. Evaluation results for comfort and safety prove applicability of the presented shock absorber. With mass of 5.8 Kg, the full scale model will be harvesting 176–227 W of peak energy for suspension velocities of 0.2–0.4 m/sec.

2. Material and Methods

2.1. Overview of HESA. Arrangement of HESA is shown in Figure 1. The shock absorber uses linear generator, fluid damper, and linkage mechanism for motion amplification. Linkage mechanism amplifies shock absorber displacement and operates the linear generator with increased velocity and displacement. Linkage mechanisms are efficient in motion amplification [18, 19]. These are relatively inexpensive and with lower mass of the links, dynamics of the system is not significantly affected. With the presented mechanical motion amplification, HESA has shown significant improvement in harvesting efficiency. Flow area between piston and cylinder of the fluid damper is varied to ensure stroke dependent damping force. Flow area is slightly larger to ensure lower fluid damping intensity near equilibrium position of the shock absorber. For its further movement, the flow area is reduced to obtain higher damping intensity. Suspension stroke for lower fluid damping intensity corresponds to the most frequent rattle movement of the shock absorber. This value ranges from 12 to 50 mm, for a car travelling on city roads [23].

Linear generator assembly comprises two concentric permanent magnets (PMs) columns, as illustrated in Figure 2. With superimposition of magnetic flux, double column structure used in the prototype results in more improved flux density than that of single column. Magnets are assembled with same polarities facing each other. Two-phase armature coil is moving in the radial air gap between the two columns. Central rod and the outer tube support the magnet and pole array. Coil assembly is wound on a nylon tube to eliminate eddy currents. There are no eddy currents even in the outer tube, since it does not move relative to the magnets.

2.2. Numerical Computation of Electromechanical Parameters. The HESA is analyzed for acceleration transmissibility, force transmissibility, tire discomfort, and energy harvested by using modified quarter car model, as shown in Figure 1. Amplification mechanism connected between sprung and unsprung mass is driving the linear generator placed in horizontal direction. Suspension spring and the fluid damper are connected between the two masses. Unsprung mass has a spring related to tire stiffness between itself and the lower mass. Electromagnetic damping force and inertia of the linear generator act along links in the mechanism. Vertical components of these forces affect transmissibility of the shock absorber and are considered in the numerical model.

Equations of motion for the quarter car model are given as

$$\begin{aligned}\ddot{z} = {} & \frac{k_s}{m_1}\left(y_{(t)} - z_{(t)}\right) + \frac{b_{s(t)}}{m_1}\left(\dot{y}_{(t)} - \dot{z}_{(t)}\right) \\ & - \frac{F_{\mathrm{lg}(t)}}{m_1}\left(\sin\theta_{(t)}\cos\theta_{(t)}\right) \\ & - \frac{m_{\mathrm{lg}}\ddot{u}_{(t)}}{m_1}\left(\sin\theta_{(t)}\cos\theta_{(t)}\right),\end{aligned} \tag{1}$$

$$\begin{aligned}\ddot{y} = {} & \frac{k_s}{m_2}\left(z_{(t)} - y_{(t)}\right) + \frac{b_{s(t)}}{m_2}\left(\dot{z}_{(t)} - \dot{y}_{(t)}\right) \\ & + \frac{F_{\mathrm{lg}(t)}}{m_2}\left(\sin\theta_{(t)}\cos\theta_{(t)}\right) + \frac{m_{\mathrm{lg}}\ddot{u}_{(t)}}{m_1}\left(\sin\theta_{(t)}\cos\theta_{(t)}\right) \\ & - \frac{k_t}{m_2}\left(y_{(t)} - x_{(t)}\right),\end{aligned} \tag{2}$$

where $z_{(t)}$ is the sprung mass displacement, $y_{(t)}$ is the unsprung mass displacement, $x_{(t)}$ is the tire displacement, $F_{\mathrm{lg}(t)}$ is the braking force on the armature coils in the linear generator, m_{lg} is the mass of the linear generator, $\ddot{u}_{(t)}$ is the acceleration of the linear generator, k_s is the suspension stiffness, b_s is the fluid damping coefficient, and k_t is the tire stiffness.

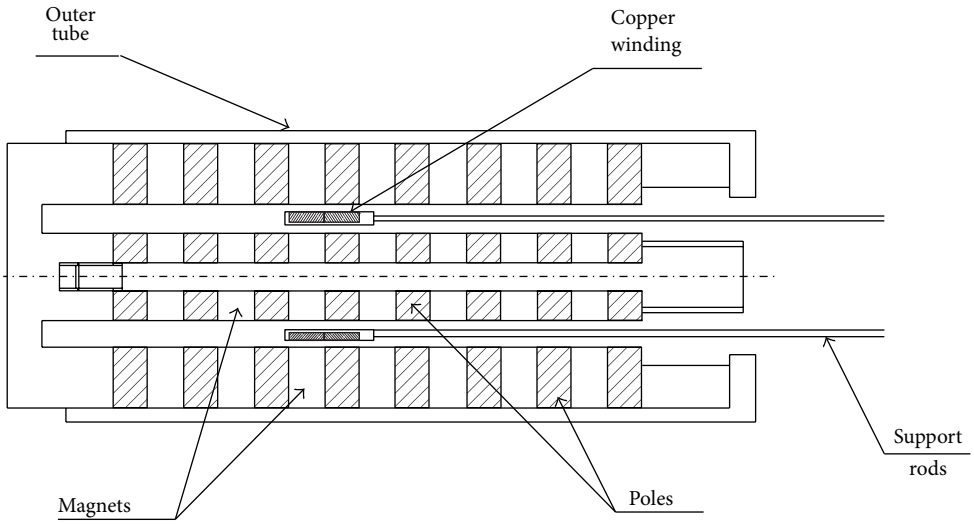

Figure 2: Schematic diagram of linear generator.

Armature coil displacement in the linear generator is given as

$$u = \frac{h-(y-z)}{2\tan\left(\sin^{-1}\left((h-(y-z))/2l\right)\right)} - \left(\frac{1}{2}\sqrt{4l^2-h^2}\right), \quad (3)$$

where h is the distance between sprung and unsprung mass at equilibrium position and l is the amplification mechanism link length.

Armature coil moves with the following velocity relative to the magnets:

$$\dot{u} = \frac{(\dot{y}-\dot{z})}{2\tan\left(\sin^{-1}\left((h-(y-z))/2l\right)\right)}. \quad (4)$$

Voltage generated in each of the armature phase is computed with the use of finite difference method and is given as

$$E_{(t)} = \frac{(\dot{y}-\dot{z})}{2\tan\left(\sin^{-1}\left((h-(y-z))/2l\right)\right)} \times \frac{4D_{\text{av}}N_p k_{\text{fill}}}{d_w^2}\int B_{g_{(t)}}\,dA, \quad (5)$$

where $B_{g(t)}$ is the air gap magnetic flux density, D_{av} is the armature coil average diameter, N_p is the number of coils in each phase, d_w is the armature coil copper wire diameter, and k_{fill} is the filling factor of the armature coil.

By making suitable end connections, voltage generated by each of the phase is added. Armature voltage needs to be rectified to DC for using the harvested energy in some useful application like charging the automobile battery. A switching circuit, as has been shown in Figure 3, can be used for this application, which will consist of couple of switches and a shunt resistance. In operation of HESA, when armature voltage will be greater than the battery threshold value, switch 2 will be closed and switch 1 will be open. This ensures that the harvested energy is used for charging the battery. On the other hand, for lower armature voltage switch 1 will be closed and switch 2 will be open. This will make the electrical energy dissipated into heat by passing the current through the shunt resistance, by closing switch 1. In this paper the generator is connected to the electrical load for study.

Braking force on the armature coils is given as

$$F_{\text{lg}} = \frac{\pi D_{\text{av}}N_c N_p n_p I_{(t)}}{A_c}\int B_{g_{(t)}}\,dA, \quad (6)$$

where $I_{(t)}$ is the armature current, A_c is the coil cross section area, n_p is the number of phases in the armature, and N_c is the number of copper wire turns in each phase.

Using (1) and (6), electromagnetic damping coefficient for each generator phase is given as

$$C = \left[\left(\frac{1}{2\tan\left(\sin^{-1}\left((h-(y-z))/2l\right)\right)}\frac{4D_{\text{av}}N_p k_{\text{fill}}}{d_w^2} \times \left(\sum_{i=1}^{np}\int B_{g_{(t)}}\,dA\right)\right) - \frac{npN_p L_{\text{coil}}}{(\dot{y}-\dot{z})}\frac{dI}{dt} - \frac{V_B}{(\dot{y}-\dot{z})}\right]\frac{4D_{\text{av}}N_p K_{\text{fill}}}{Rd_w^2}\int B\,dA, \quad (7)$$

where R is the total resistance, L_{coil} is the inductance of the single coil, and V_B is the battery voltage.

Equation (7) characterizes electromagnetic damping coefficient in terms of coil dimensions, copper wire parameters, opposing battery voltage, and electrical load. Inductive voltage drop and opposing battery voltage contribute

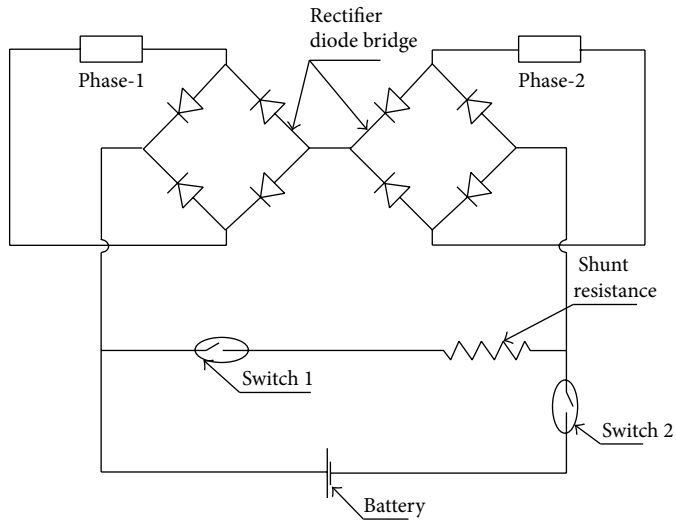

Figure 3: Switching circuit.

to mechanical nonlinearity of the damping coefficient. As observed from (7), damping coefficient is directly proportional to square of magnetic flux density. Also it improves with higher filling factor and larger average coil diameter.

Optimum choice of copper wire diameter is crucial to ensure maximum damping effect by the linear generator. With lower copper wire diameter even though voltage across the coils is higher, increased inductive and resistive drops reduce the damping effect. Whereas, with larger wire diameter, inductive and resistive voltage drops are lower, the voltage generated by the coils reduces.

RMS value of relative displacement between tire and unsprung mass has been used to evaluate tire discomfort of HESA. Zero tire discomfort means no relative displacement in tire and unsprung mass, which gives best handling. On the other hand, higher RMS relative deflection causes deterioration of road holding ability and increases tire discomfort [23].

2.3. Numerical Model of HESA. Linear generator simulation is done with FE analysis and Matlab model. Air gap in the linear generator is discretized into number of subregions. Values of magnetic flux density along these subregions are calculated with two-dimensional axisymmetric FE analysis in ANSYS 13. Magnetic flux density values along the air gap are used in Matlab Simulink model of the generator. Back EMF on the coils, resistive drop, inductive drop, opposing battery voltage, and voltage drop of rectifier diode have been taken into account in numerical simulation of the linear generator.

Numerical model of HESA is constructed in Matlab Simulink and Simscape. Quarter car simulation is based on (1) and (2), which computes performance parameters of HESA. Mechanical linkage mechanism is defined in Matlab Simscape. This linkage mechanism operates with relative displacement and velocity calculated by the quarter car model. Linear generator modeled in Simulink moves with output motion computed by the Simscape linkage mechanism. Simulink model of the linear generator calculates armature voltage, current, braking force on the coils, and harvested energy.

Fluid damper is modeled in Simscape. Numerical model of HESA consists of fluid damper, mechanical linkages, linear generator, and quarter car model. Fluid force, coil braking force, and generator inertia are analyzed and total damping force has been computed by adding these contributions. Simulations on this model are used to evaluate efficiency of the linear generator for different copper wire diameters. FE analysis and numerical model of HESA will be later used in the design of full scale version, after experimental validation with a prototype and this has been discussed in Section 3.

Figure 4 shows flow chart for the numerical model of HESA.

2.4. Prototype HESA. Harvesting systems discussed in the past literature have magnet and pole array connected to the wheel, whereas coils are connected to the vehicle body [1, 3, 6]. Voltage is induced in the coils as they move relative to the magnets. Double increase of coil relative velocity gives quadratic rise in the harvested energy with the damping force increasing by twofold. Thus, both harvesting efficiency and damping effect of the linear generator can be significantly improved by operating the linear generator with amplified velocity.

Presented HESA uses linkage mechanism for amplification of relative velocity between sprung and unsprung mass. It has displacement sensitive fluid damper as additional dissipative element. Within suspension stroke of 34 mm, the fluid damper in the prototype offers lower damping intensity, whereas for further movement, reduction in the fluid flow area increases damping force. This proposed fluid damper has symmetric damping characteristics in compression and rebound stroke.

Proposed linear generator has dimensions of the poles identical to those of the magnets. Equal diameters of pole and magnet ensure that the armature coil will come across

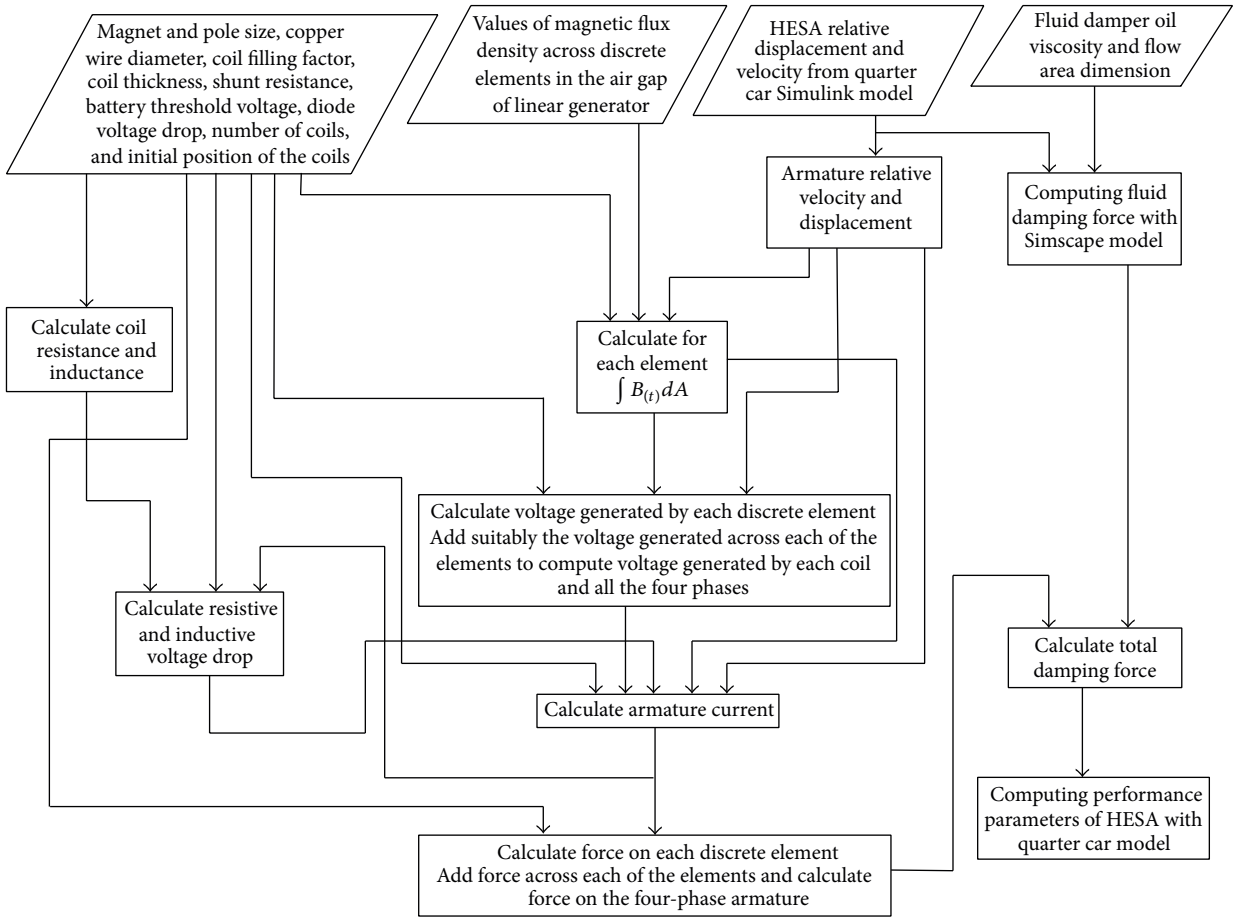

Figure 4: Flow chart for numerical model of HESA.

most of flux lines in air gap. Also, with similar values of magnet and pole thickness, average radial flux density in the air gap is 64% to its peak value. High permeable AISI 1018 steel has been used for the poles. Central column of magnet and spacers is secured in position by stainless steel guide rod. Outer magnet and poles are stacked inside an aluminum cover. Since stainless steel rod and aluminum cover have higher magnetic reluctance, these do not pull the flux. This helps to increase magnetic flux density in the air gap. External diameter of the outer magnets is chosen based on suitability of using the shock absorber in general vehicles. Inner magnets are chosen to achieve radial air gap width of 6 mm. Lower air gap width not only generates greater electrical energy but also implies manufacturing difficulty. The armature has two-phase construction with 0.2 mm copper wire diameter and 150 number of turns in each phase. Prototype linear generator has 120 mm of working stroke.

Central stainless steel rod is extended beyond the magnet column and is used to locate the linear generator. The generator is supported on one side of the linkage mechanism, whereas coils are being carried by the other side. Linkage mechanism has been fabricated with 8 mm square cross section mild steel bars.

Design details of linear generator and fluid damper used in prototype HESA are summarized below:

(i) magnet material: C 5-Ferrite;

(ii) dimensions of outer magnet: 60 × 32 × 8 mm (outer diameter, inner diameter, and thickness);

(iii) dimensions of inner magnet: 20 × 6 × 8 mm;

(iv) fluid flow area up to 34 mm stroke of the damper: 150.33 mm^2;

(v) fluid flow area beyond 34 mm stroke of the damper: 138.56 mm^2;

(vi) amplification mechanism link length: 180 mm;

(vii) effective stiffness of the prototype HESA springs: 13332 N/m.

2.5. Experimental Setup. Numerical model of HESA is validated with experimentation performed on the prototype, with details as discussed in the earlier section. The experimental setup used in the present study is shown in Figures 5 and 6. Test setup is designed to measure armature voltage, motion transmissibility, force transmissibility, sprung mass acceleration, and RMS value of relative displacement between lower mass and the unsprung mass. Armature voltage is an important parameter since both harvested energy and electromagnetic damping force depend on it. Sinusoidal excitations of amplitude of 11.2 mm are given to the lower

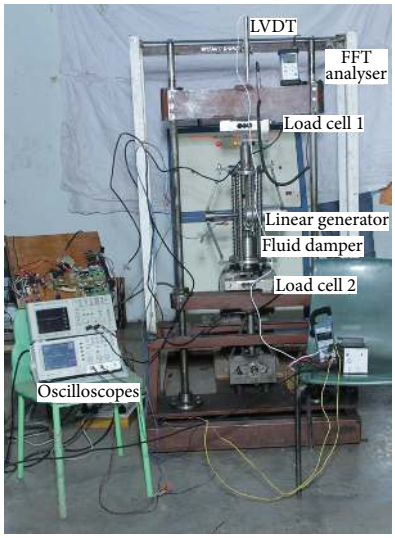

Figure 5: Experimental setup for prototype HESA.

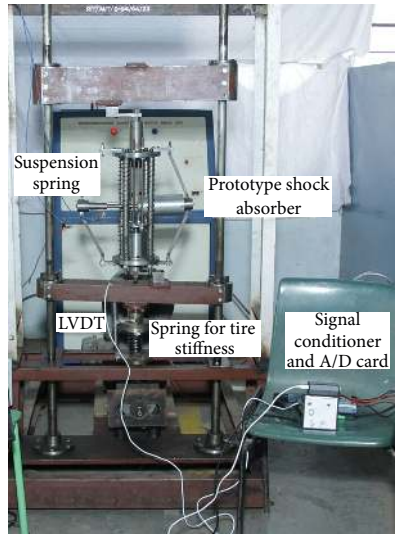

Figure 6: Experimental setup to validate tire discomfort.

mass. Within the test frequency range, excitation velocity is 0.1 to 0.7 m/sec. This is close to normal and high bump velocities of the shock absorber, which are up to 0.4 m/sec and 0.8 m/sec, respectively [23].

Two degrees of freedom test setup, shown in Figure 5, measure motion transmissibility, sprung mass acceleration, force transmissibility, and armature voltage for 5Ω of load resistance. Force transmissibility is measured by load cells located above unsprung mass and below sprung mass. Oscilloscope is used to capture voltage waveforms of the load cells and armature coils. LVDT correlated damping force and armature voltage waveforms to the shock absorber displacement. Svantek FFT meter (SVN958) with accelerometer measures acceleration and displacement at the sprung mass.

To validate tire discomfort, another test setup, as shown in Figure 6, is established. This has the lower mass and the unsprung mass connected by a spring of stiffness of 106 KN/m. As shown in Figure 6, the setup operates with 3 degrees of freedom and uses a LVDT to measure relative displacement between the unsprung mass and the lower mass. Data acquisition hardware DT9812 along with QuickDAQ2013 software is used to record the relative displacement signal in the computer.

3. Results and Discussion

Voltage across the armature coils in the prototype is given as

$$E_{(t)} = \sum_{i=1}^{2} \left[\left(\frac{(\dot{y} - \dot{z})}{2 \tan\left(\sin^{-1}\left((h - (y - z))/2l\right)\right)} \frac{4 D_{\text{av}} N_p k_{\text{fill}}}{d_w^2} \times \int B_{g_{(t)}} dA \right) - \left(2 L_{\text{coil}} \frac{dI}{dt} \right) - \left(R I_{(t)} \right) \right]. \quad (8)$$

As seen from (8), frequency of generated voltage differs from that of the input excitations. Frequency of voltage depends on interval of magnetic flux reversal in addition to that of the input excitations. With lesser values of magnet and pole thickness, voltage waveform frequency increases. Since armature velocity, magnetic flux density, and number of turns in the magnetic field decide voltage across the armature coils, voltage waveform shows nonuniform peaks.

Figure 7(a) shows simulation and experimental voltage waveform at 3.16 Hz excitation frequency. With the linear generator operating in horizontal direction, the waveform shows peak voltage of 80 mV. The RMS values of the simulation and experimental waveforms are observed to be 42 mV and 36 mV, respectively. Numerical simulations are performed with the linear generator located vertically and operating without amplification. In this case, peak and RMS voltage are estimated to be 12 mV and 7.9 mV, respectively. This shows that the presented amplification mechanism improves generator voltage to 660%. It is observed that in comparison to the linear generator operating without amplification, voltage waveform frequency of the prototype HESA is significantly higher.

At 3.66 Hz excitation frequency, peak voltage across the armature winding is 120 mV as seen from Figure 7(b). The RMS values of experimental and simulation voltage waveforms are 56 mV and 59.4 mV, respectively.

Figure 7(c) shows numerical simulation results for variation of generator voltage along the linear generator displacement at 5.16 Hz. With 8 mm thick magnets and poles, armature coil in the air gap comes across flux reversal at 16 mm distance. This makes voltage waveform have peaks and valleys spaced at 16 mm. It is observed that with the presented amplification mechanism, coil movement in the generator is not identical to the input motion. Coil displacement during upward movement of the shock absorber is higher than that of downward movement. This behavior is on account of asymmetric output from the linkage mechanism, which makes the generator harvest greater voltage for upward movement of the shock absorber.

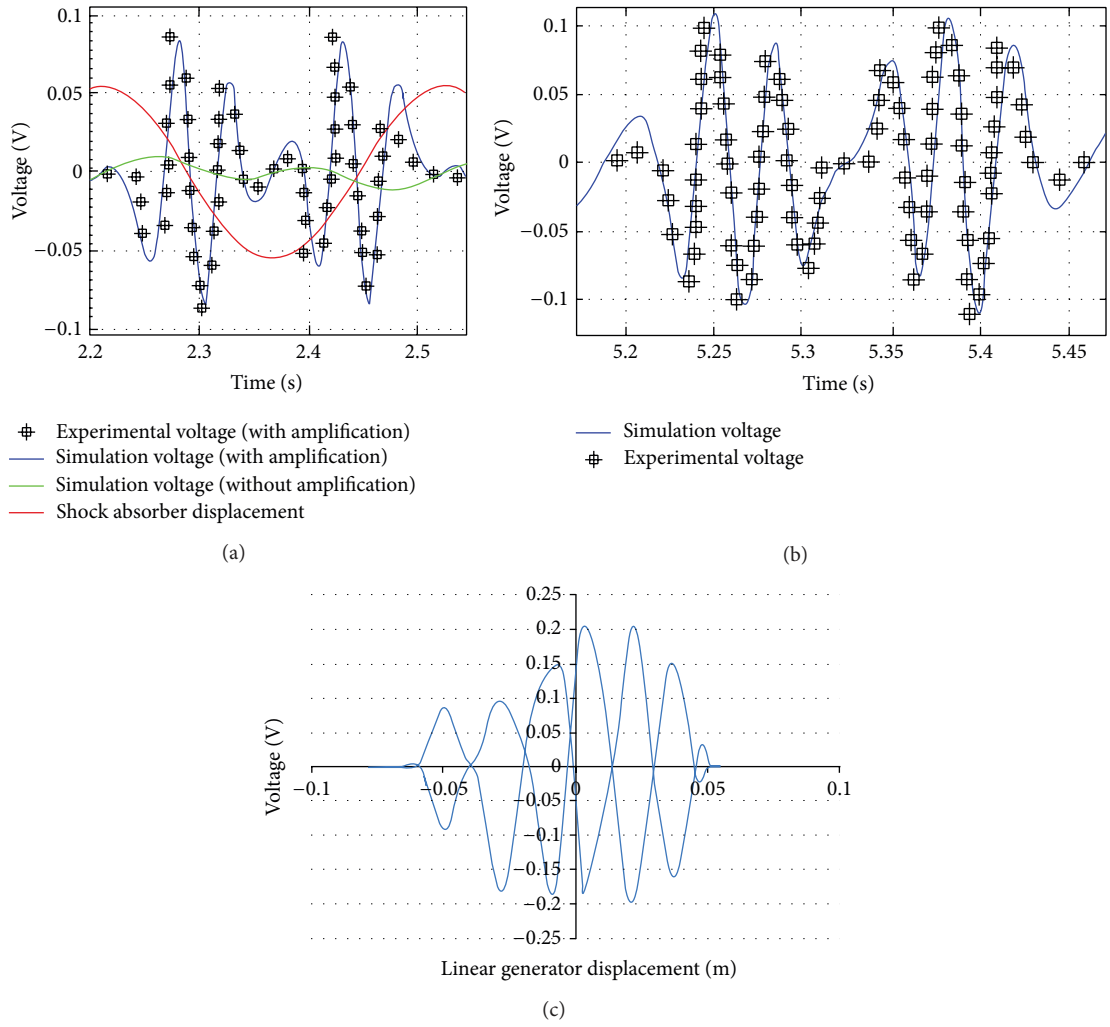

FIGURE 7: Comparison of voltage plots for the prototype.

Damping force in the prototype HESA will include fluid damping force and vertical component of braking force on the armature coils, which is given as

$$F_{\text{damping}} = \left[\frac{6\pi\upsilon\rho t_p D p^4}{D_c\left(D_c - D_p\right)^3}\left(\dot{z} - \dot{y}\right)\right] + \left[\left(\frac{4D_{\text{av}}N_c I_{(t)}}{d_w^2}\int B_{g_{(t)}}dA\right)\left(\sin\theta_{(t)}\cos\theta_{(t)}\right)\right], \quad (9)$$

where υ is the kinematic viscosity of oil in the damper, ρ is the oil density, t_p is the piston thickness, D_c is cylinder diameter, and D_p is the piston diameter.

Inertia of the linear generator acts on the sprung and unsprung mass along the linkages. It is observed that its effect is insignificant in force transmissibility up to 4 Hz. Figure 8(a) shows damping force-displacement curve for the prototype at 5 Hz. Numerical simulation on the prototype without accounting the generator inertia shows that energy dissipated per cycle is 2.15% lesser when this effect is considered. As observed, up to 5 Hz generator inertia is out of phase with sprung mass acceleration and acts in direction of the damping forces. However, since the generator acceleration changes its phase with respect to the sprung mass acceleration, it is observed that energy dissipated, with accounting the generator inertia, increases slightly by 0.5% at 6 Hz. Generator inertia affects transmissibility in the prototype because of lower sprung mass. However, for the full scale model with sprung mass of 350 kg, its effect is insignificant.

Figure 8(b) summarizes simulation and experimental results for voltage and energy, with two degrees of freedom model. Good correlation has been obtained between measured and simulated results. The derived numerical model of the linear generator exhibits maximum error of 8.6% in voltage estimation.

Experimental and numerical simulation results for motion and acceleration transmissibility are illustrated in Figure 8(c). Response characteristics of the prototype HESA are of similar nature to that of fluid shock absorbers. Motion transmissibility is observed to increase with frequency and is maximum within resonance frequency. Maximum acceleration of 4.6 m/s^2 is observed at 5.2 Hz. As observed

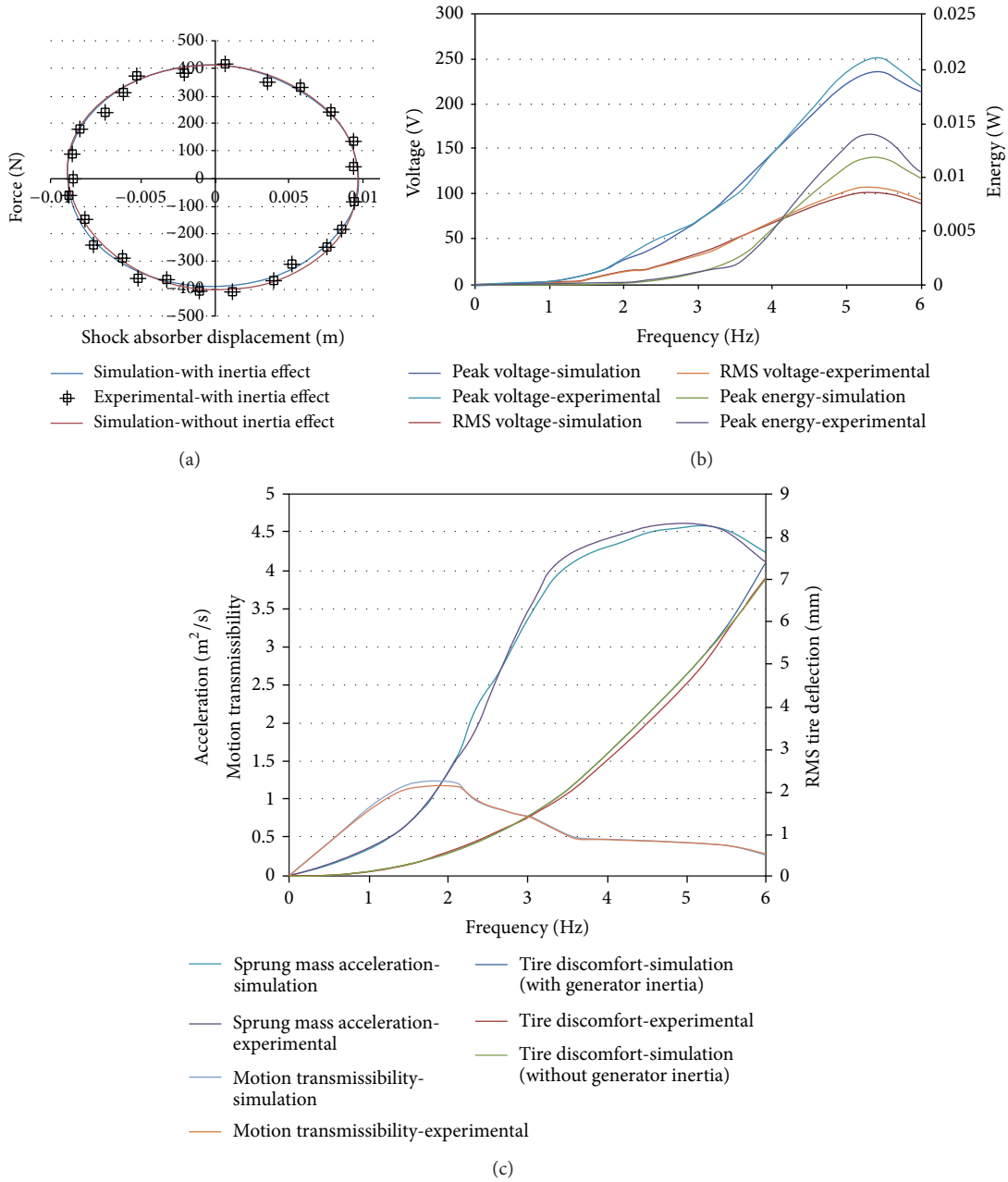

FIGURE 8: Comparison of numerical analysis and experimental results for prototype HESA performance.

from Figure 8(c), numerical simulation results for performance of the prototype HESA are in close agreement to that of the experimental findings.

Figure 8(c) shows the RMS values of relative displacement between lower mass and the unsprung mass, computed with 3 degrees of freedom model, as discussed earlier. As seen from Figure 8(c), the tire discomfort is observed to increase with frequency. Numerical simulations are performed to compute tire discomfort without accounting the generator inertia. It is observed that the inertia does not affect tire discomfort up to 4 Hz. However, beyond 4 Hz, simulation shows lesser tire discomfort, when the inertia component is neglected. Generator inertia increases tire discomfort because of asymmetric variation of acceleration along the shock absorber displacement.

Electromagnetic damping force on the armature is given as

$$F_{\mathrm{lg}} = \left[\left(\frac{(\dot{y}-\dot{z})}{2\tan\left(\sin^{-1}\left((h-(y-z))/2l\right)\right)}\frac{4D_{\mathrm{av}}N_p k_{\mathrm{fill}}}{d_w^2} \times \left(\sum_{i=1}^{np}\int B_{g_{(t)}}\,dA\right)\right) - npN_p L_{\mathrm{coil}}\frac{dI}{dt}\right] \times \left[\frac{\pi D_{\mathrm{av}}N_p n_p}{R}\right]\left[\int B\,dA\right]. \quad (10)$$

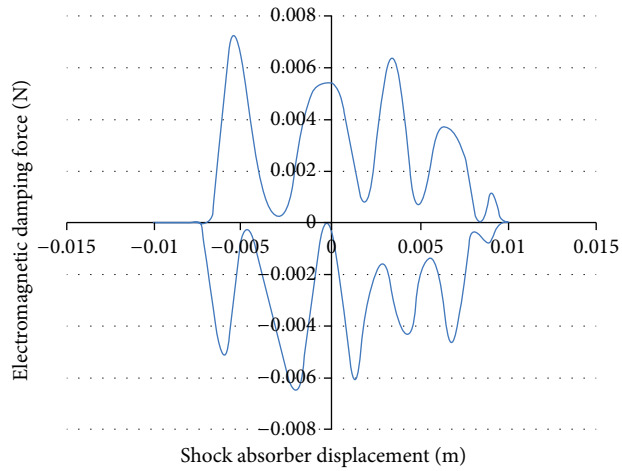

Figure 9: Electromagnetic damping force along the shock absorber displacement at 5 Hz.

As observed from (10), electromagnetic damping force depends on the coil relative velocity and magnetic flux reversal spacing, and its frequency differs from the excitation frequency. As shown in Figure 9, electromagnetic damping force on the armature coil varies significantly across the armature stroke with On-Off effect. This finding is in consonance with Oprea et al. [1] and Li et al. [11], who have highlighted variation in electromagnetic damping force along the damper displacement. For using a shock absorber in automobile suspension, this aspect is not desirable. Use of thicker magnet and pole thickness reduces the difference in the two frequencies. In full scale model, magnet and pole thickness are derived for maximum braking effect on the armature coils.

In case of fluid dampers, damping force curve has a closed loop, which is elliptical in shape [22]. However, in case of linear generators, variation in the electromagnetic damping force will reduce amount of energy dissipated per cycle. This will result in higher acceleration transmissibility and greater variation in the forces transmitted to the tire. This aspect limits the application of linear generators as the only dissipative element in vehicle shock absorbers.

Motion amplification and harvesting efficiency of the presented shock absorber are better for shorter length of links in the amplification mechanism. With link lengths of 180 mm, maximum velocity amplification of 8.2 has been achieved in the prototype. However, while designing the mechanism for a vehicle shock absorber, link length should be selected in accordance with the most frequent displacement in the shock absorber. At peak displacement of about 25 mm from the mean position of shock absorber, the mechanism should just close.

Energy recovery is the most important characteristic of the presented shock absorber. The prototype is given sinusoidal displacement excitations with peak amplitude of 11.2 mm. Input power is calculated from work done to displace the mass in one cycle as

$$E_{\text{in}} = \left(m_1 + m_2 + m_3\right) g \int X_o \sin\left(2\pi f t\right) dt, \tag{11}$$

where X_o is the input displacement amplitude and f is the excitation frequency.

Efficiency of the amplification mechanism is computed based on the displacement of the linear generator. Output power is calculated as

$$E_{\text{out}} = m_{\text{lg}} g \int u_{(t)} dt. \tag{12}$$

With 0.05 N m of torque to account for the kinetic friction at each of the revolute joint, the mechanism works with 49.78% efficiency (at 4 Hz, peak velocity 0.276 m/sec). When length of links in the amplification mechanism is increased by 40 mm, the efficiency reduces to 47.40%. Harvesting efficiency of HESA further depends on the linear generator design and is discussed further.

After validating the numerical model of prototype HESA, the design is modified for an automotive application to support mass of 350 kg. To improve harvesting efficiency and damping effect of the linear generator, rare earth magnets (Nd-Fe-B, N-35 grade) are proposed in the full scale model.

Details of the full scale model are given as follows:

(i) dimensions of outer magnets and poles: (OD × ID × Thickness) 60 × 32 × 8 mm;

(ii) dimensions of inner magnets and poles: 20 × 6 × 8 mm;

(iii) armature coil: 0.57 mm wire diameter with 0.75 filling factor;

(iv) suspension spring stiffness: 22 KN/m;

(v) threshold voltage for operating the switching circuit: 14 V;

(vi) battery opposing voltage: 12 V;

(vii) shunt resistance: 5 Ω;

(viii) amplification mechanism links: material-EN24 with rectangular cross section (6 × 3 mm).

Copper wire diameter affects damping and harvesting efficiency of the linear generator as has been discussed earlier. However, current rating of the wire has been taken care of while selecting coil configuration for the full scale model. Automobile shock absorbers are designed with damper asymmetry to improve road holding performance while travelling over potholes [23, 24]. Damper asymmetry ensures higher extension force to avoid free drooping of the wheel. In accordance with this, damping coefficient of full scale HESA in compressions and extension stroke is computed with damper asymmetry of 30/70. HESA dissipates vibration energy with fluid and electromagnetic damping. Damping coefficient of the fluid damper, along its stroke length, proposed for the full scale model is illustrated in Figure 10(a). Amplification mechanism will operate the linear generator for 25 mm displacement from the mean position. Electromagnetic damping force will be effective only for this stroke length. Therefore fluid damping coefficient is higher, beyond 25 mm displacement from the mean position as seen from Figure 10(a). To account for asymmetric velocity

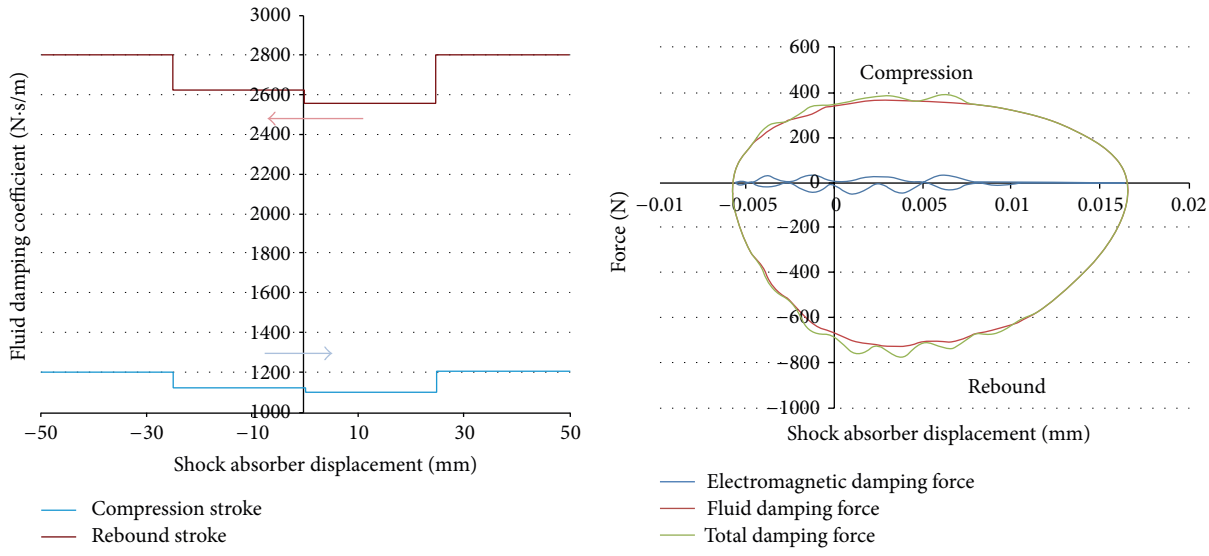

FIGURE 10: Variation of damping coefficient and damping force along the shock absorber displacement.

amplification, fluid damping intensity is kept slightly lower for upward stroke than that of downward stroke.

Energy harvested by the linear generator is given as

$$E_{\text{out generator}} = \int E_{(t)} I_{(t)} dt. \tag{13}$$

With the presented configuration of the linear generator, harvesting efficiency in HESA will be 19.25% (at 4 Hz, peak velocity 0.276 m/sec). With 20% reduction in fluid damping coefficient, harvesting efficiency improves to 20.81%. However, tire discomfort increases by 15.66% and peak acceleration transmitted to the occupants drops down by 13.6%. On the other hand, for 20% increase in the fluid damping coefficient, harvesting efficiency reduces to 13.11%. Tire discomfort comes down by 12.81% and peak acceleration transmitted to the sprung mass increases by 14.28%. Fluid damping coefficient should be chosen for better harvesting efficiency, with due consideration of ride and comfort in the vehicle.

Configurations of electromagnetic shock absorbers discussed in the past literature have magnet and pole array connected to the wheels whereas coils are carried by vehicle body [1, 8, 15]. In the present case, both comfort and handling are likely to be affected since the braking force on the coils with significant variation along the shock absorber displacement is directly transmitted to the sprung and unsprung mass. For the presented HESA, with linear generator located horizontally, vertical component of the braking force on the armature coils acts through the linkages. At 4 Hz, maximum braking force on the coils will be 148 N whereas vertical component of this force affecting the shock absorber performance will be 42 N. Damping in HESA is done primarily by the fluid damper, which has smoother variation of the damping force along the shock absorber displacement, as has been shown in Figure 10(b). Variation of total damping force in HESA is observed to be less uneven than that of electromagnetic shock absorbers discussed in the published literature [1, 11]. In case of winding failure, HESA will display lower force level, but it will still provide significant damping effect.

Damping force of the electromagnetic devices presented in the past literature reports significant variation with change in the electrical load resistance [11, 12]. Amati et al. have observed that for suspension velocity of 0.4 m/sec, 20 Ω change in load resistance will vary the damping force by 500 N. However, for the present design of HESA, this change of resistance will affect the damping force by 38.8 N. It can be seen that when HESA is used for some auxiliary application (e.g., battery charging), its damping performance will not significantly change with the electrical load.

Figure 11(a) shows peak and RMS values of energy harvested by HESA. Low to medium bump velocities, for an automobile suspension, range from 0.1 to 0.4 m/sec. For this range of velocity, proposed HESA will harvest 75–227 W of peak energy. Higher inductive losses in the armature coils will reduce energy harvested by HESA beyond 8 Hz.

Numerical analysis is performed to compare performance of full scale HESA and fluid shock absorber (with mean damping coefficient of 2000 N s/m and damper asymmetry factor of 0.4). In comparison to the fluid shock absorber, HESA shows minor increment in motion transmissibility, acceleration transmissibility, and RMS tire deflection as can be seen from Figure 11(b). As discussed earlier, generator inertia affects transmissibility in case of the prototype. However simulations performed on the full scale model show that the generator inertia does not affect motion and acceleration transmissibility.

Numerical simulations are performed for analyzing effect of magnet and pole thickness on the generator damping and energy recovery. For 8 mm thick magnet and poles, peak average radial magnetic flux density in the air gap is 0.60 Tesla (T). With 8 mm thick magnets and pole thickness reduced

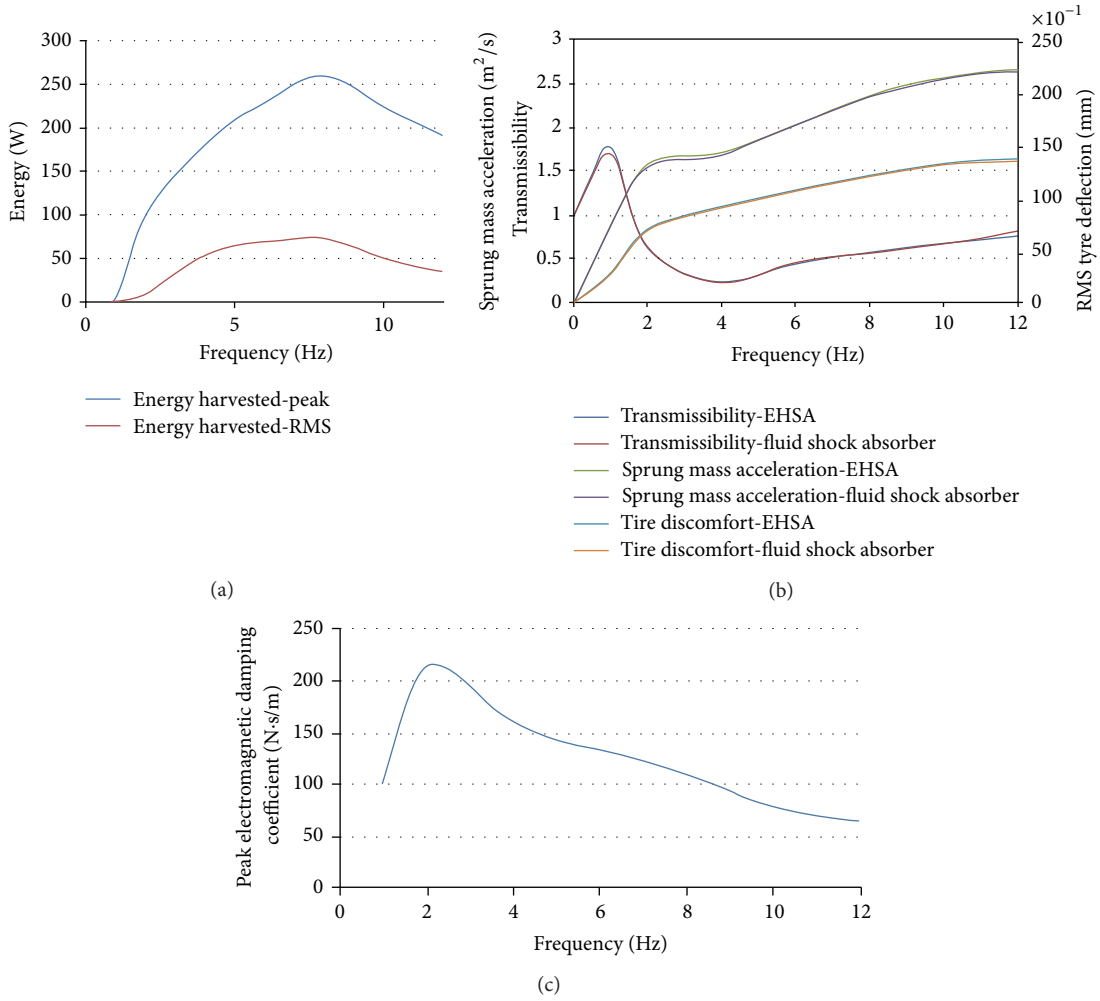

Figure 11: Numerical simulation results on full scale HESA.

to 6 mm, peak average radial magnetic flux density in the air gap improves to 0.72 T. However, energy dissipated per cycle by the linear generator is 81 % to that of the generator configuration, with 8mm thick magnet and poles (at 4 Hz, peak velocity 0.276 m/sec). Also RMS value of the harvested energy reduces to 67%. On the other hand, when pole thickness is reduced to 6 mm, RMS value of the harvested energy drops to 58% and energy dissipated becomes 78 %, to that of the generator configuration with 8 mm thick magnet and poles.

Proposed HESA is also compared with passive fluid dampers for cost and weight. Passive monotube and twin-tube fluid dampers cost 80 US$ and 200 US$, respectively [25]. Price of HESA is estimated to be around 360 US$. Higher cost of HESA is attributed to expensive rare earth magnets. Moreover since density of the magnets is three times that of steel, HESA is marginally heavier than fluid shock absorbers. Weight of twin-tube fluid dampers is 4.8 Kg (Gabriel make, AM-0177, vehicle: Tata Motors, India, Indica V2), whereas CAD weight of full scale HESA is 5.8 Kg. Even though cost and weight of HESA are moderately high, it will improve overall fuel efficiency of the vehicle.

Figure 11(c) illustrates variation of peak electromagnetic damping coefficient for the range of frequency. As seen from this figure, electromagnetic damping coefficient is nonlinear in nature. Higher inductive losses reduce electromagnetic damping coefficient at higher frequencies.

Since vehicle vibrations are seldom harmonic, numerical simulation is performed on the model of HESA with broadband excitations. For broadband analysis, armature voltage generated in each phase is determined as

$$V = 2\pi^2 X_o D_{av} N_c N_p \cos(2\pi f t)\left(f + t\frac{df}{dt}\right)\int B_{(t)}\,dA. \quad (14)$$

Equation (14) implies that broadband voltage should be greater than that of harmonic voltage for increase in the frequency. Also inductive drop will be different under harmonic and broadband excitations. Since both output power and damping force depend on the voltage, HESA performance will be affected by broadband excitations. Analysis performed at 4 Hz shows that RMS electromagnetic damping force for broadband excitations differs by 1.3%. Similarly harvested energy in both the cases will vary by 2.2%. This aspect will

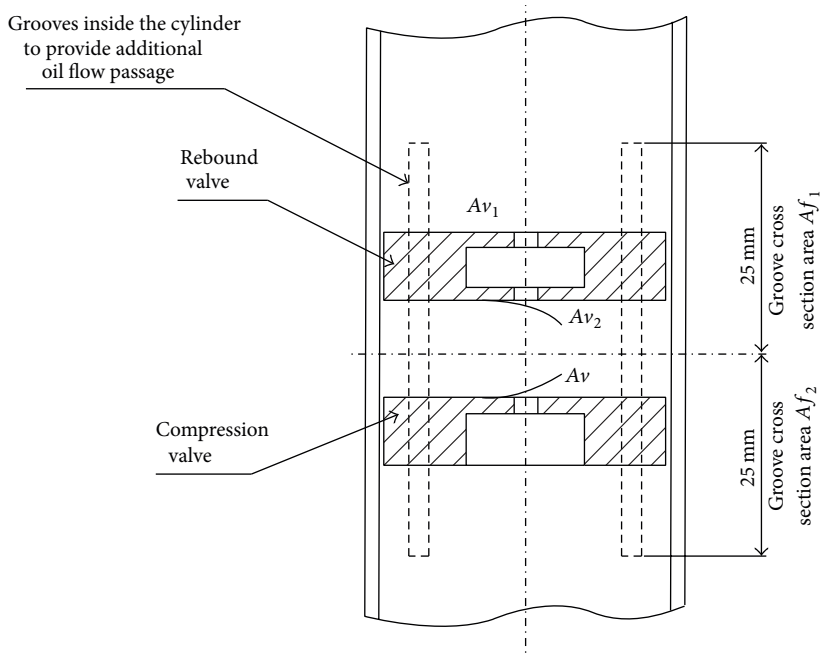

Figure 12: Valve model for the fluid damper.

add to the nonlinear nature of the electromagnetic damping force.

Damping coefficient illustrated in Figure 10(a) can be achieved with the combination of orifices in piston and longitudinal grooves inside the cylinder.

The proposed damper asymmetry requires different configurations of valves in compression and rebound stroke. Valve model for the damper is shown in Figure 12.

During compression and rebound stroke, oil will pass through piston valves and cylinder grooves. Local throttle losses of the oil flow are analyzed to compute the fluid damping coefficient. When piston valve pressure exceeds the cracking limit, the spring loaded valve will lift to give additional flow passage. This causes increased energy dissipation at higher suspension velocities. Further details of orifice opening area, valve cracking pressure, and cylinder groove details are given as follows:

(i) details for the longitudinal groove inside the cylinder:

- (a) cross sectional area above the piston mean position (Af_1): 1.4 mm$^{2;}$
- (b) cross sectional area below the piston mean position (Af_2): 1.2 mm^2;
- (c) cumber of grooves (n_f): 4;

(ii) compression valve details:

- (a) minimum flow area for each opening (A_{vc}): 2.8 mm^2;
- (b) number of flow path (nv_{rc}): 8;
- (c) valve cracking pressure (P_{cfrc}): 1.8 MPa;
- (d) maximum flow path area for each opening ($Avc_{\max}$): 4.6 mm^2;

(iii) rebound valve details:

- (a) flow area for each opening (Av_{r1}): 3.8 mm^2;
- (b) number of flow path (nv_{r1}): 4;
- (c) minimum flow area for each opening (Av_{r2}): 4.2 mm^2;
- (d) number of flow path (nv_{r2}): 8;
- (e) valve cracking pressure (P_{cfrr}): 1.2 MPa;
- (f) maximum flow path area for each opening ($Avr_{2\max}$): 6.2 mm^2.

Longitudinal grooves inside the cylinder will provide additional flow path for the oil, which helps to achieve the required damping strategy. The cylinder should have thickness of about 1.7 mm and the grooves can be manufactured by shaping operation [23]. To incorporate higher damping coefficient in rebound stroke, this valve consists of two orifices connected in series as has been shown in Figure 12.

Based on analytical computation discussed in the available reference [26], damping coefficient of the fluid damper assuming laminar flow at the orifices can be written as follows.

For compression stroke

$$C = \frac{A_{comp}^2 \upsilon \rho}{2C_{DL}\left(n_{vc}A_{vc}D_{Hvc} + n_f A_f D_{Hf}\right)}. \tag{15}$$

For rebound stroke

$$C = \frac{A_{\text{rebound}}\,(\text{dP})}{\left(\dot{y} - \dot{z}\right)}. \tag{16}$$

Pressure difference (dP) across the valve is calculated with the following equation:

$$A_{\text{rebound}}\left(\dot{y}-\dot{z}\right) = \frac{0.081 n_f A_f D_{Hf}}{\upsilon\rho}\,(\text{dP}) + \frac{0.081 n_{vr1} A_{vr1} D_{Hvr1}}{\upsilon\rho} \times \left[(\text{dP}) - (\text{dP})\,\frac{n_{vr1} A_{vr1} D_{Hvr1}}{n_{vr2} A_{vr2} D_{Hvr2}}\right], \quad (17)$$

where D_{Hcv} is the orifice hydraulic diameter at area A_{vc}, A_f is the flow area at the cylinder slot, ρ is the density of the oil, D_{Hf} is the hydraulic diameter at cylinder slots, D_{Hvr1} is the orifice hydraulic diameter at area A_{vr1}, and D_{Hvr2} is the orifice hydraulic diameter at area A_{vr2}.

FE analysis indicates that maximum stress in the amplification mechanism links will be limited to 38 MPa, which is much lesser than yield limit of the material. Also maximum working temperature of the shock absorber will be much lower than Curie temperature of FeNdB magnets, which is 310°C [6]. To fully demagnetize FeNdB material, external magnetic field of equal polarity needs to be applied. When used in the shock absorber, these magnets will not have significant loss in their strength, since demagnetization of the magnet material is less than 3% for 50°C rise in temperature [6].

Full form HESA can be fitted in rear suspension of a car having front engine. The proposed linear generator and the fluid damper would not be placed in the same plane. Rather amplification links and the generator will be offset from the damper and suspension spring axes, and also it will be away from the tires. This is to ensure that these parts do not interfere with each other. The configuration consisting of generator with outer diameter of 60 mm, maximum working stroke of 400 mm, and 180 mm long amplification links can be used for a midsize car. With the proposed arrangement there will be minor reduction (~3%) in rear storage space. The use of longer amplification links with larger generator diameter is recommended for better power output; however, these dimensions may be constrained by space availability.

Presented HESA is compared for weight and regenerated energy with electromagnetic energy harvesters reported in the past literature. Li et al. achieved peak power of 67.5 W and average power of 19.2 W from four-rotary design electromagnetic shock absorbers [11]. Electromagnetic shock absorber developed by Zuo and Zhang dissipates peak energy of 110 W, for 0.27 m/s suspension velocity [24]. Amati et al. achieved peak damping coefficient of 2500 N s/m in an electromagnetic shock absorber [12]. The shock absorber uses ball screw arrangement with a rotary generator. CAD calculated weight of the shock absorber is 5 Kg. Zuo et al. harvested 2–8 W of energy with a prototype electromagnetic energy harvester for suspension velocities of 0.25–0.50 m/sec. Zuo et al. estimate that 16–64 W of energy can be the harvested form full scale energy harvester for this range of suspension velocity [2].

4. Conclusion

This paper presents design, analysis, and validation of a novel regenerative shock absorber with linear generator and fluid damper. Mechanical amplification used in the presented shock absorber does not substantially increase weight and inertia of the system. Moreover, it results in significant magnification of the armature relative velocity. Numerical simulation shows that harvesting efficiency of HESA is better than that of systems reported in the past literature.

Electromagnetic damping coefficient is observed to be nonlinear in nature with inductive drop and opposing battery voltage as its contributing factors. Simulations with broadband excitations show minor variation in HESA performance than that of harmonic analysis.

Detailed dynamic analysis supported by experimental validation shows that it is feasible to develop HESA that can fulfill shock absorber and power generation objectives simultaneously.

Proposed HESA can be used in vehicles with sufficient space to accommodate mechanical linkage mechanism. It can be fitted in light and heavy commercial vehicles with chassis frame and also in rear suspension of midsized car with integrated body and chassis.

Performance of the proposed HESA can be further improved with use of low weight, high quality magnets. Also, the presented scheme of integrating velocity amplification with electromagnetic and fluid damping can be extended to other applications in vibration isolation.

Conflict of Interests

The authors declare that there is no conflict of interests regarding the publication of this paper.

References

[1] R. A. Oprea, M. Mihailescu, A. I. Chirila, and I. D. Deaconu, "Design and efficiency of linear electromagnetic shock absorbers," in *Proceedings of the 13th International Conference IEEE Optimization of Electrical and Electronic Equipment (OPTIM '12)*, pp. 630–634, Brasov, Romania, 2012.

[2] L. Zuo, B. Scully, J. Shestani, and Y. Zhou, "Design and characterization of an electromagnetic energy harvester for vehicle suspensions," *Smart Materials and Structures*, vol. 19, no. 4, Article ID 045003, pp. 1–10, 2010.

[3] L. Zhen and X. Wei, "Structure and magnetic field analysis of regenerative electromagnetic shock absorber," in *Proceedings of the WASE International Conference on Information Engineering (ICIE '10)*, pp. 152–155, Beidaihe, China, August 2010.

[4] Y. Kawamoto, Y. Suda, H. Inoue, and T. Kondo, "Modeling of electromagnetic damper for automobile suspension," *Journal of System Design and Dynamics*, vol. 1–3, pp. 524–534, 2007.

[5] K. Nakano, Y. Suda, and S. Nakadai, "Self-powered active vibration control using a single electric actuator," *Journal of Sound and Vibration*, vol. 260, no. 2, pp. 213–235, 2003.

[6] B. Ebrahimi, M. B. Khamesee, and F. Golnaraghi, "Permanent magnet configuration in design of an eddy current damper," *Microsystem Technologies*, vol. 16, no. 1-2, pp. 19–24, 2010.

[7] R. B. Goldner and P. Zerigian, "Electromagnetic linear generator and shock absorber," Patent 6952060, Tufts College, Medford, Mass, USA, 2005.

[8] I. Zador, *Rear earth and high temperature superconducting permanent magnet synchronous tube motor/generator optimization for the components of the car suspension system [Ph.D. thesis]*, Budapest University of Technology and Economics, Budapest, Hungary, 2008.

[9] S. Ohashi and T. Matsuzuka, "Basic characteristics of the linear synchronous generator using mechanical vibration," *IEEE Transactions on Magnetics*, vol. 41, no. 10, pp. 3829–3831, 2005.

[10] O. D. Paz, *Design of electromagnetic shock absorber [M.S. thesis]*, B. S. Universidad, 2004.

[11] Z. Li, L. Zuo, G. Luhrs, L. Lin, and Y. Qin, "electromagnetic energy-harvesting shock absorbers: design, modeling, and road tests," *EEE Transactions on Vehicular Technology*, vol. 62, no. 3, pp. 1065–1074, 2013.

[12] N. Amati, A. Festini, and A. Tonoli, "Design of electromagnetic shock absorbers for automotive suspensions," *Vehicle System Dynamics*, vol. 49, no. 12, pp. 1913–1928, 2011.

[13] Z. Fang, X. Guo, L. Xu, and H. Zhang, "Experimental study of damping and energy regeneration characteristics of a hydraulic electromagnetic shock absorber," *Advances in Mechanical Engineering*, vol. 2013, Article ID 943528, 9 pages, 2013.

[14] P. S. Zhang, *Design of electromagnetic shock absorbers for energy harvesting from vehicle suspensions [M.S. thesis]*, Stony Brook University, 2010.

[15] C. T. Liu and W. P. Lin, "Feasibility investigations of an integrated suspension/generation system for vehicle shock damping applications," in *Proceedings of the 9th International Symposium on Linear Drives for Industry Application*, pp. 1–4, Hangzhou, China, 2013.

[16] L. V. Blarigan, P. Danzl, and J. Moehlis, "A broadband vibrational energy harvester," *Applied Physics Letters*, vol. 100, Article ID 253904, pp. 1–5, 2012.

[17] P. R. Ouyang, W. J. Zhang, and M. M. Gupta, "Design of a new compliant mechanical amplifier," in *Proceedings of the ASME International Design Engineering Technical Conferences and Computers and Information in Engineering Conference (DETC '05)*, pp. 1–10, Long Beach, Calif, USA, September 2005.

[18] Z. Hadas, C. Ondrusek, and V. Singule, "Increasing sensitivity of vibration energy harvester," in *Smart Sensors, Actuators, and MEMS 4th*, vol. 7362, pp. 1–8, May 2009.

[19] I. Zeimpekis, I. Sari, and M. Kraft, "Characterization of a mechanical motion amplifier applied to a MEMS accelerometer," *Journal of Microelectromechanical Systems*, vol. 21, no. 5, pp. 1032–1042, 2012.

[20] H. C. Huang and R. J. McNamara, "The efficiency of the motion amplification mechanism with viscous damper," *Earth Quake Engineering and Engineering Vibrations*, vol. 8, pp. 521–536, 2009.

[21] D. Sekulić and V. Dedović, "The effect of stiffness and damping of the suspension system elements on the optimization of the vibrational behaviour of a bus," *International Journal For Traffic and Transport Engineering*, vol. 1, no. 4, pp. 231–244, 2011.

[22] C. Zhou, Y. Liu, and Y. Cai, "Characteristic simulation of telescopic shock absorber," in *Proceedings of the IEEE 7th International Asia Conference on System Simulation and Scientific Computing (ICSC '08)*, pp. 159–163, Chengdu, China, October 2008.

[23] J. D. Dixon John Wiley and Sons, London, UK, 2nd edition, 2007.

[24] L. Zuo and P. S. Zhang, "Energy harvesting, ride comfort and road handling of regenerative vehicle suspensions," *ASME Journal of Vibration and Acoustics*, pp. 1–8, 2012.

[25] B. Ebrahimi, M. B. Khamesee, and F. Golnaraghi, "Eddy current damper feasibility in automobile suspension: modeling, simulation and testing," *Smart Materials and Structures*, vol. 18, pp. 1–12, 2009.

[26] Y. A. Cengel and J. Cimbala, *Fluid Mechanics Fundamentals and Applications*, McGraw-Hill, New York, NY, USA, 2006.